Results in Physics 49 (2023) 106526

Contents lists available at ScienceDirect

Results in Physics

journal homepage: www.elsevier.com/locate/rinp

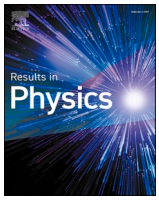

Accurate dipole radiation model for waveguide grating couplers

Zhen Liu *, Mohamed A. Ettabib, James S. Wilkinson, Michalis N. Zervas

Optoelectronics Research Centre, Zepler Institute for Photonics and Nanoelectronics, University of Southampton, Southampton SO17 1BJ, UK

ARTICLE INFO

Keywords:
Waveguide grating coupler
Multilayer interference
Dipole radiation
Coupling efficiency
Guided mode

ABSTRACT

An analytical theoretical model for the waveguide grating coupler is developed and applicable to practical deep gratings. The grating-assisted input coupling efficiency is calculated by considering the reciprocal out-coupling problem. The deep grating structure is modelled as an optical layer filled with polarization dipole sources, and the scattered fields are then calculated using the associated Green's functions and taking into account the multiple reflections and interference from the adjacent layers. The joint loss between the grating region and the waveguide is also considered. Comparison with numerical simulations shows very good agreement and validates the accuracy of the analytical model. The model explicitly describes the importance of multilayer interference of the scattered fields and guided-mode joint loss on the total grating-assisted coupling efficiency and can be used for practical waveguide grating coupler design with negligible computation workload.

Introduction

Waveguide grating couplers (WGCs) are proving to be essential components for coupling light from fiber/free space into integrated waveguide circuits and have found increasingly widespread use in areas such as silicon photonics [1] and, more recently, in bio-medical sensing [2]. Over the years, WGCs have attracted extensive research related to their underlying physical mechanisms and efficiency optimization. The WGC input coupling efficiency (CE) is usually treated in an analytical manner by considering its reciprocal problem of out-coupling or output scattering [3–5]. However, the output scattering analytical models are usually based on a rather restrictive assumption that the grating depth is small [3], which makes the modelling inaccurate in a number of practical situations. For more accurate calculations, numerical simulation is the mainstream approach for WGC optimization [2,6].

However, full numerical models suffer from several shortcomings. Firstly, the WGC CE is affected by a number of factors, and a full optimization taking into account all contributing parameters can result in prohibitively long computing times. Secondly, numerical searching for the most efficient solutions could converge on a local optimum, especially when the parameter space is large. Finally, important underlying physical mechanisms can be obscured, and significant physical insight can be lost.

In this paper, an accurate theoretical model for WGCs without the assumption of small grating depth is developed and compared to numerical simulations. The physical mechanisms defining the WGC CE are clarified, showing that multiple reflections from adjacent interfaces of each WGC layer can affect the overall CE.

Theoretical model

The grating is inscribed on the surface of a three-layer waveguide, with refractive indices $n_a - n_f - n_s$, and core thickness h (see Fig. 1). To bypass the complicated direct input-coupling problem, the model considers the "reciprocal" out-coupling problem and uses a Green-function formalism for surface optics to calculate the strength of the various scattering orders [7].

Reciprocal approach for WGC

Following Ref. [3–5], the "direct" grating-assisted input coupling problem is dealt with by considering first the "reciprocal" out-coupling problem. The reciprocity of WGC is shown in Fig. 1, which contains two aspects. The first aspect of the reciprocity is the reciprocal propagating guided waves and scattered orders, as shown Fig. 1(a) and (b), marked by solid double line in green ("reciprocal" output coupling) and red ("direct" input coupling). The second reciprocity is the field distributions in the input and output coupling cases, which is shown in Fig. 1(c).

In the "reciprocal" case, as shown in Fig. 1(d), the out-coupled n^{th}-scattering orders fulfill the relation:

$$k_z = \beta + nK_g (n = \pm 1, \pm 2, \ldots), \tag{1}$$

* Corresponding author.
E-mail address: zhen.liu@soton.ac.uk (Z. Liu).

https://doi.org/10.1016/j.rinp.2023.106526
Received 23 March 2023; Received in revised form 6 May 2023; Accepted 6 May 2023
Available online 9 May 2023

where $k_z = k_a\sin(\theta_n^a) = k_s\sin(\theta_n^s)$, $k_{a(s)} = n_{a(s)}k_0$, $K_g = 2\pi/d$, d is the grating period, n is the scattered order, $\theta_n^a(\theta_n^s)$ is the scattering angle in medium a(s), and β is the propagation constant in the four-layer (n_a-n_g-n_f-n_s) waveguide. The grating period is adjusted so that there is only one scattered order in the substrate (s) and cover (a) layer. The "direct" and "reciprocal" problems are connected through the Lorentz reciprocity theorem [5], which dictates that only waves travelling in exactly opposite directions should be considered. Oppositely propagating waves are only the incident (−1 scattered order) wave and the coupled (incident) waveguide mode in the "direct" ("reciprocal") cases. The corresponding power pairs are denoted (P_i^*, P_{-1}^s) and (P_0^*, P_0) (see Fig. 1 (a)-(c)). It can be shown that the WGC CE can be given by [5]:

$$\frac{P_0^*}{P_i^*} = \left[\int_L g(z)h(z)dz\right]^2 \frac{P_{-1}^s}{P_0}, \tag{2}$$

where $g(z)$ is the normalized exponentially decaying profile of the output field, and $h(z)$ is the normalized Gaussian profile of the input field (see Fig. 1(c)). Power conservation requires that the total power P_0 is the summation of all the scattered powers, so $P_{-1}^{s(a)}/P_0 = \alpha_{-1}^{s(a)}/\alpha_{tot}$, where $\alpha_{tot} = \alpha_{-1}^s + \alpha_{-1}^a$ [3], and $g(z) = g_0\exp(-\alpha_{tot}z)$. $g(z)$ is the aperture function [5] normalized such that $\int_{-\infty}^{+\infty}[g(z)]^2dz = 1$.

Dipole radiation in optical interfaces

To make it applicable to "thick" gratings, we replace the grating region with a uniform layer with a volume-averaged refractive index n_g and thickness that equals to the grating depth σ, following the approach in Ref. [8], as shown in Fig. 2. To be specific, the average index n_g for the grating layer is calculated as $n_g = \left(\int_V n^2(r)/Vdr\right)^{0.5}$ within a single period, i.e. $V \in (0 > z > -d, 0 > y > -\sigma)$, following Ref. [9]. The grating layer is typically much thicker than the random roughness in Ref. [8], so the reflection in the grating layer must be considered. We next consider the fields generated by infinitesimal scattering-dipole sheets within the "average index" layer and take into account multiple reflections from the adjacent layer interfaces, utilizing the transfer matrix method [10] (see Fig. 2 (b)), which will be detailed below. We finally integrate the entire "average index" grating layer thickness to obtain the total scattered fields.

To calculate the scattering coefficients α_{-1}^s and α_{-1}^a, we consider an infinitesimal scattering-dipole sheet within the grating region (n_g) (see Fig. 2). A similar approach has been adopted by Schmid et al. for modelling scattering loss from the rough surface of waveguides [8]. In this case, the wave equation takes the form:

$$\nabla^2\boldsymbol{E} + n^2(y)k_0^2\boldsymbol{E} = 4\pi k_0^2\boldsymbol{P}, \tag{3}$$

where k_0 is the wavevector in free space and $n(y)$ is the refractive index in each layer shown in Fig. 2, and $\mathbf{P}$ is the additional polarization source due to the infinitesimal scattering-dipole sheet at y_0. The modal field for the four-layer structure can be found from the homogeneous solution of Eq. (3). The simple transfer matrix method [10] is applied to obtain the propagating constant and modal field distribution in this work. Using the shift theorem [11], the polarization $\mathbf{P}$ induced by the modal electric field $\mathbf{E}(y_0, z) = \mathbf{E}(y_0)\exp(\beta z)$ at the point y_0 is Fourier transformed and takes the form [8]:

$$P(y_0, k_z) = \frac{\left(n_g^2 - n_a^2\right)}{4\pi\sigma}\tilde{s}(k_z - \beta)\left(\hat{x}\hat{x} + \frac{n_a^2}{n_g^2}\hat{y}\hat{y} + \hat{z}\hat{z}\right)E(y_0), \tag{4}$$

where $\tilde{s}(k)$ is the Fourier transform of the grating surface profile and $\hat{x}$, $\hat{y}$, $\hat{z}$ are the coordinate unit vectors. This study focuses only on the TE mode, so only the $\times$ component of the electric field is considered. Fourier transforming the square-wave grating profile, $\tilde{s}$ is expressed as $\tilde{s}(k_z - \beta) = \sigma\Sigma_{n=-\infty}^{+\infty}c_n 2\pi\delta(k - 2\pi n/d)$, where $c_n = Dsinc(nD)$ is the

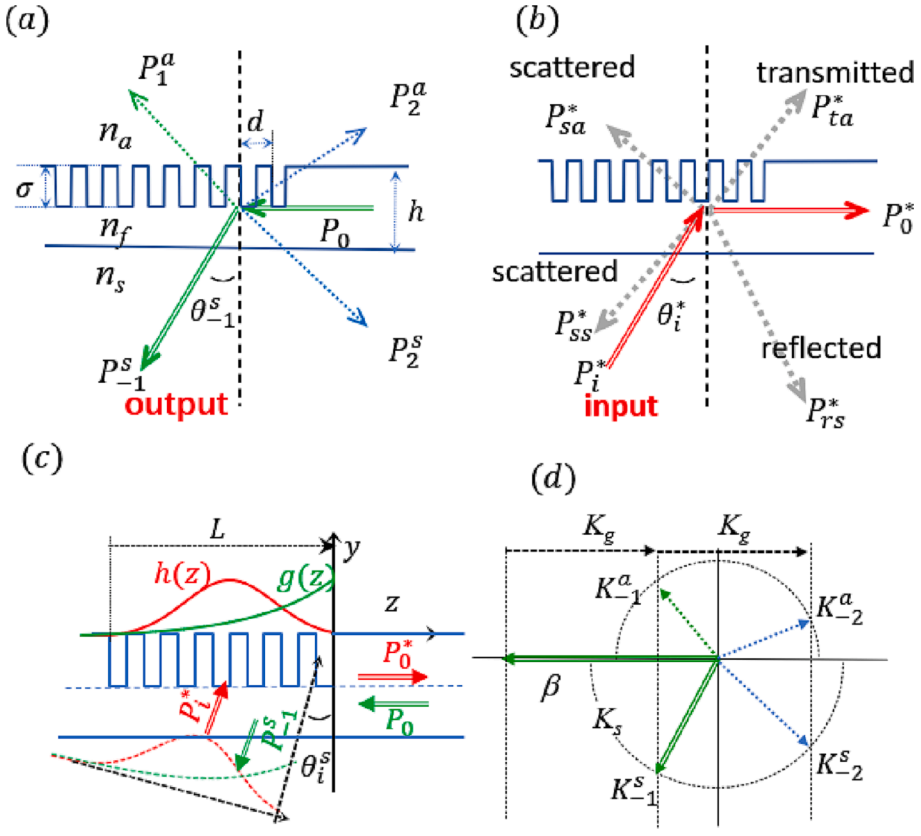

Fig. 1. Reciprocity of input/output coupling of WGC: propagation directions for the (a) "reciprocal" (green) case and (b) "direct" (red) case. The refractive indices of cladding, core and substrate are n_a, n_f, and n_s, respectively, and the etched grating depth is σ with a period of d; (c) field distributions for the "direct" (red) and "reciprocal" (green) cases. (d) Vector diagram showing the scattering orders for the "reciprocal" (green) cases. (For interpretation of the references to colour in this figure legend, the reader is referred to the web version of this article.)

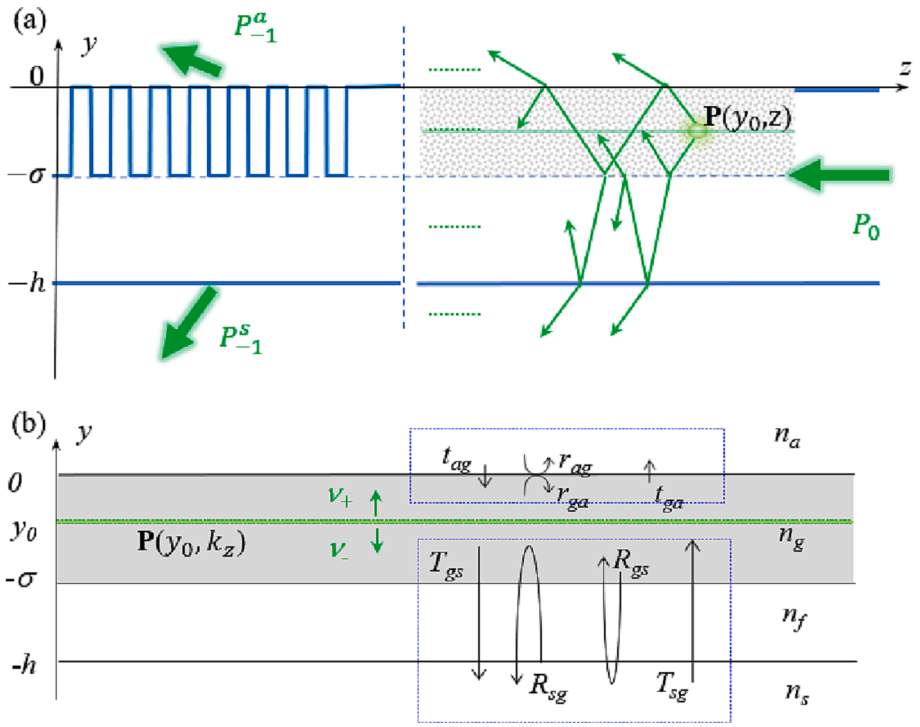

Fig. 2. Dipole radiation model of WGC: (a) The grating is replaced by a special layer of average index n_g filled with infinitesimal scattering-dipole sheets, with radiation exiting the multilayer structure after multiple reflections. (b) Illustration of multilayer reflection/transmission with the dipole source in the grating layer, in terms of transfer matrix method.

Fourier coefficient for the square wave with duty cycle D. Therefore, the polarization in a TE mode WGC is simplified to

$$\boldsymbol{P}(y_0,k_z)=\frac{\left(n_g^2-n_a^2\right)}{2}\sum_{n=-\infty}^{+\infty}c_n\delta\left(k+\frac{2\pi n}{d}\right)\boldsymbol{E}_x(y_0). \tag{5}$$

The scattered field due to the source polarization inside an optical layer is found with the use of surface Green's functions, the introduction of vectors $e_q(y)=\left[E_{q+}e^{+ik_{yq}y},E_{q-}e^{-ik_{yq}y}\right]^T$ and the use of the discontinuity-source vector method [12], namely:

$$\begin{aligned} e_a(0)&=M_{ag}M_g(-y_0)e_g\left(y_0^+\right)\\ e_g\left(y_0^-\right)&=M_g(y_0+\sigma)\boldsymbol{M}_{gs}e_s(-h), \end{aligned} \tag{6}$$

where the vector $e_a(0)=\left[\mathbf{E}_a^+,0\right]^T$ and $e_s(-h)=\left[0,\mathbf{E}_s^-e^{ik_{ys}h}\right]^T$, in which the $\mathbf{E}_a^+$ and $\mathbf{E}_s^-$ are the electric field in the cladding and substrate generated by the source polarization $P(y_0,k_z)$ at point y_0 (no incident fields from $\pm\infty$ are assumed). The matrices M_{xy} and M_x are the regular transfer matrices detailed in Ref. [10,12] and Appendix. Specifically, the subscript xy denotes transfer from layer x to y, while the single-lettered subscript indicates transfer in a specific layer, where there is only the phase shift due to propagation. $\boldsymbol{M}_{gs}=M_{gf}M_fM_{fs}$ is the composite *g-s-f* layer transfer matrix, which can also be expressed in terms of the *g-f-s* layer total reflectivities (R_{gs}, R_{sg}) and transmissivities (T_{sg}, T_{gs}) [12] (see also Fig. 2 (b)) The field at the upper limit $e_g\left(y_0^+\right)$ and lower limit $e_g\left(y_0^-\right)$ of the source have the relation expressed as, $e_g\left(y_0^+\right)=[v_+,-v_-]^T+e_g\left(y_0^-\right)$, where $v_\pm$ is given as [8,12]:

$$v_\pm=\frac{2\pi ik_0^2}{k_{yg}}\cdot\boldsymbol{P}(y_0,k_z), \tag{7}$$

where k_{yg} is the y component of the wavevector and given as $k_{yg}^2=k_0^2n_g^2-k_z^2$. After some simple linear algebra (see Appendix), the up and down going electric fields due to the infinitesimal source polarization sheet at y_0 can be found as

$$\begin{aligned} E_s^-(y_0,k_z)&=\frac{T_{gs}e^{+ik_{yg}\sigma}\left(v_+r_{ga}e^{-i\Phi_0}+v_-e^{+i\Phi_0}\right)}{1-r_{ga}R_{gs}e^{+i2k_{yg}\sigma}}\\ E_a^+(y_0,k_z)&=\frac{t_{ga}e^{+ik_{yg}\sigma}\left(v_+e^{-ik_{yg}\sigma}e^{-i\Phi_0}+v_-R_{gs}e^{+ik_{yg}\sigma}e^{+i\Phi_0}\right)}{1-r_{ga}R_{gs}e^{+i2k_{yg}\sigma}}, \end{aligned} \tag{8}$$

where $t_{ga}(r_{ga})$ is the transmittance (reflectance) across interface *ag*, and $T_{gs}(R_{gs})$ is the total transmittance (reflectance) across the composite g-f-s layer structure (see Fig. 2 (b)). $\Phi_0=k_{yg}y_0$ is the phase shift due to propagation from y_0 to 0.

By substituting Eqs. (5) and (7) into (8), $\mathbf{E}_a^+$ and $\mathbf{E}_s^-$ can be written as function of modal field $\mathbf{E}_\mathbf{x}(y_0)$ in the wavevector domain. The scattered field due to source polarization at y_0 can be found by Fourier transforming $\mathbf{E}_a^+(y_0,k_z)$ and $\mathbf{E}_s^-(y_0,k_z)$ back into the real space. Similar approach has been followed by Payne and Lacey when modeling the random scattering from waveguides with rough surfaces [7].

The total scattered electric fields in the substrate (s) and cladding (a) areas are obtained by integrating the contributions of the infinitesimal source polarization sheet over the entire grating layer, and expressed as:

$$\begin{aligned} \boldsymbol{E}_{ns}^-&=\frac{c_nk_0^2\left(n_g^2-n_a^2\right)e^{+ik_{yg}\sigma}}{2k_{yg}\left(1-r_{ga}R_{gs}e^{+i2k_{yg}\sigma}\right)}\left[\int_{-\sigma}^{0}f_s(y_0)\boldsymbol{E}_x(y_0)dy_0\right]\\ \boldsymbol{E}_{na}^+&=\frac{c_nk_0^2\left(n_g^2-n_a^2\right)e^{+ik_{yg}\sigma}}{2k_{yg}\left(1-r_{ga}R_{gs}e^{+i2k_{yg}\sigma}\right)}\left[\int_{-\sigma}^{0}f_a(y_0)\boldsymbol{E}_x(y_0)dy_0\right], \end{aligned} \tag{9}$$

where $f_s(y_0)=\left(r_{ga}e^{+i\Phi_0}+e^{i\Phi_0}\right)$, $f_a(y_0)=\left(e^{-ik_{yg}\sigma}e^{-i\Phi_0}+R_{gs}e^{+ik_{yg}\sigma}e^{+i\Phi_0}\right)$. It should be stressed that the terms $f_s(y_0)$, $f_a(y_0)$ and $F(\sigma)=\left[1-r_{gs}R_{gs}\exp(i2k_{yg}\sigma)\right]$ express the effects of multiple reflections from the interfaces adjacent to the thick grating layer. The impact of multiple reflections on scattering has also been discussed in Ref. [3] following a different approach applicable to "shallow" gratings without treating the grating as a specific layer.

The scattered powers into the substrate and cladding can now be calculated from the corresponding scattered fields given by Eq. (9). The guided power in the grating region is calculated by $P_0 = \beta/\omega\mu\int_\infty |E_x|^2 dy$. Note that β and E_x refer to the propagation constant and the modal field distribution in the four-layer (n_a-n_g-n_f-n_s) grating region. Calculation of the scattering coefficients and consequently of the aperture function g(z) results in the calculation of the grating coupling efficiency $\eta_g = P_0^*/P_i^*$, through Eq. (2). Since we consider deep gratings, the four-layer (n_a-n_g-n_f-n_s) waveguide optical characteristics (β, Ex) can be substantially different to the ones of the initial three-layer (n_a-n_f-n_s) waveguide (β', E_x'). To account for the impact of the discontinuity between the grating and waveguide regions, we also consider the modal conversion efficiency at this joint, defined as $\eta_j = \left|\int_\infty E_x E_x' dy\right|^2 / \left(\int_\infty |E_x'|^2 dy \int_\infty |E_x|^2 dy\right)$. In this case, the total grating/waveguide coupling efficiency is given by $\eta_g^t = \eta_g \eta_j = \left(P_0^*/P_i^*\right)\eta_j$. The joint loss is given by $\alpha_j = 1 - \eta_j$.

Results and discussion

To validate the theoretical model, we compared it with our previously published numerical results based on vectorial 2D-Finite-Difference Time-Domain simulations using Lumerical FDTD Solutions [2]. The WGC is configured as follows: the grating is etched on the waveguide core with SiO_2 substrate and air cladding. The grating profile is regular uniform square-wave-shaped with a 50% duty cycle and 50 μm length. The incident light with 785 nm wavelength is launched from the substrate with the angle in the substrate $\theta_{sub} = 5.5^o$. The incident light has a Gaussian profile with a beam width of 25 μm. The etching depth and period of the grating are optimized for maximum CE. In the numerical model, the CE is calculated by solving the Maxwell equation for the whole structure when searching the optimal grating etch depth (e) and period (p). Particle swarm optimization, combined with a nested sweep of p and e, is used for this purpose. The numerical optimization is conducted on a supercomputer and takes hours to produce the results shown in Fig. 3. For the theoretical model, the running time is a few tens of seconds on a personal computer to produce much more data points, using the Brent algorithm [13] provided by the SciPy [14] package as a default searching method.

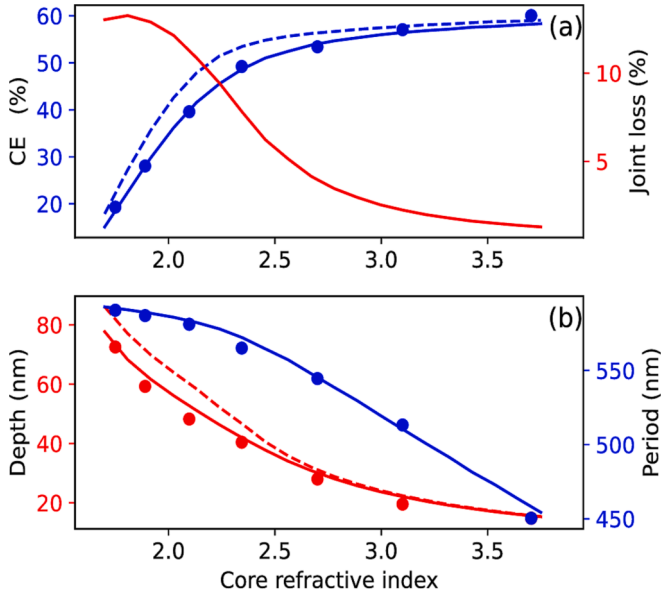

Fig. 3. CE and WGC parameters for different core indices, with core thickness selected to maximize the surface intensity; (a) CE on the left y-axis in blue and joint loss on the right y-axis (b) WGC etch depth (left axis) and grating period (right axis). Dots: numerical from Ref. [2], solid line: theoretical, dashed line: theoretical without joint loss. (For interpretation of the references to colour in this figure legend, the reader is referred to the web version of this article.)

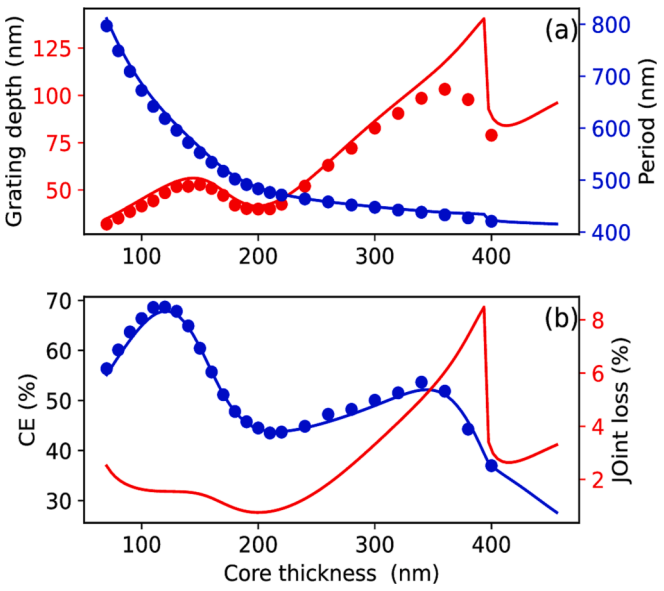

Fig. 4. Total CE and WGC parameters for different Si core thicknesses; (a) WGC etch depth (left axis-red) and grating period (right axis-blue), (b) CE (left axis–blue) and joint loss (right axis-red). Solid lines: theoretical result; dots: numerical results from Ref. [2]. (For interpretation of the references to colour in this figure legend, the reader is referred to the web version of this article.)

To further validate the theoretical model, we have compared the total CE and WGC parameter variation as a function of core thickness and compared them again to numerical data from Ref. [2]. The grating configuration and beam profile remain unchanged, except for the core material being Si at the wavelength of 1300 nm. The results are summarized in Fig. 4. Fig. 4 (a) plots the WGC etch depth (left axis-red) and grating period (right axis-blue), and Fig. 4 (b) plots the total CE (left axis

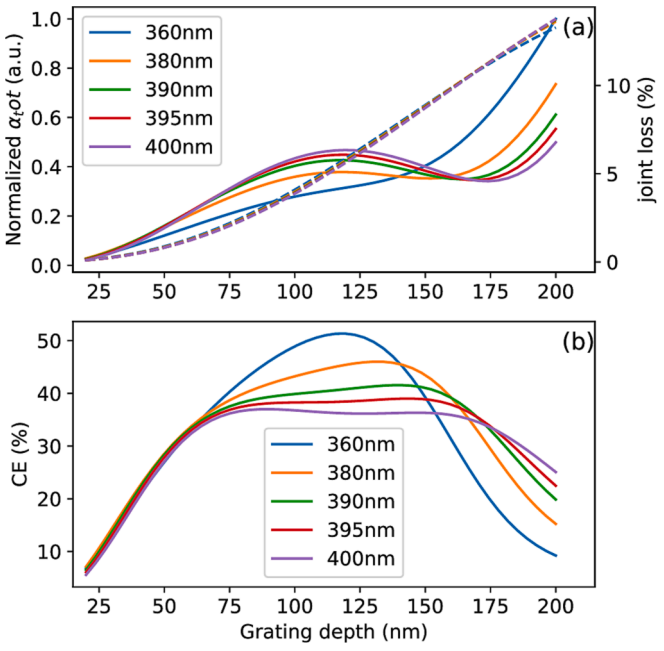

Fig. 5. (a) Normalized attenuation coefficient α_{tot} (left axis – solid lines), and joint loss (right axis – dashed lines) as a function of etch depth; (b) total CE as a function of grating depth, for different core thicknesses.

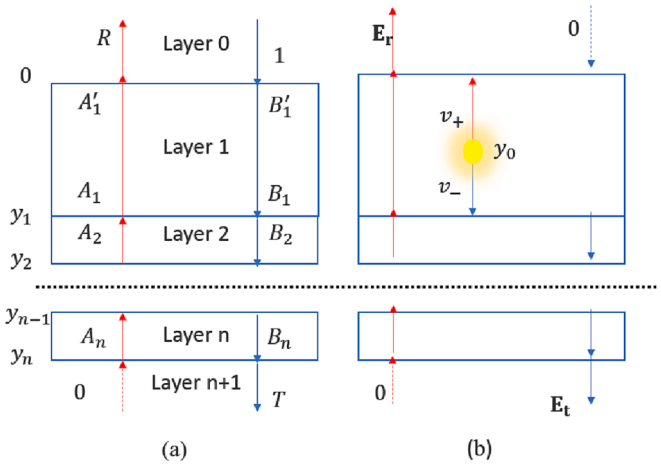

Fig. 6. Diagram for the transfer matrix for (a) standard multilayer structure with input source located outside the layers (b) multilayer structure with a special layer with a source located inside the first layer.

– solid blue line) and joint loss (right axis-red line). Also shown are the numerical results from Ref. [2] (dots).

In Fig. 3, the requirement for maximum surface intensity results in relatively thin waveguides and a monotonic increase of total CE along with a monotonic decrease of grating depth with the core refractive index. In sharp contrast, Fig. 4 shows that both the total CE and the grating depth vary non-monotonically as the core thickness increases. This is a direct result of the multiple-scattering interference effects discussed after Eq. (9). In addition, unlike Fig. 3, there is a significant discrepancy of the grating depth between the numerical and theoretical results for a core thickness around ~390 nm, although the total CEs are similar.

To clarify this discrepancy, a more detailed study on grating depth for core thickness around 390 nm is shown in Fig. 5. Fig. 5 (a) shows that the scattering strength does not increase monotonically with the etch depth, due to multilayer interference effects. At the same time, joint loss is exponentially growing. These two factors combine to "flatten" the total CE dependence on grating depth and make it multi-peaked around the core thickness of 390 nm. This renders the WGC optimization a non-convex problem, making the numerical calculation of the exact optimum grating depth very difficult. However, the "flatness" of the total CE dependence on grating depth around this core thickness results in minute differences in the returned total CE.

Conclusion

To summarize, an accurate analytical theoretical model for WGC is presented. Modelling of the grating as a modal field polarization source layer and the inclusion of joint loss between grating and waveguide are valid assumptions confirmed with numerical simulation with very good agreement. Important physical mechanisms of WGC operation are revealed with our model. The model is applicable to deep gratings and explicitly shows the impact of multiple reflections from adjacent layers in the grating region on the variation of the total CE with grating depth and core thickness. It also shows that the inclusion of the joint loss is important in calculating the total WGC CE. Such physical insights are lost when using numerical models for WGC optimization. Moreover, the analytical theoretical model is much faster than numerical models, requiring only a few minutes on a standard laptop to cover a much more extended parameter space, which makes it ideal for fast, large-scale WGC optimization. The model can also be extended to cover TM polarization operation and more general grating geometries, such as gratings with "non-square teeth" and tilted gratings.

CRediT authorship contribution statement

Zhen Liu: Methodology, Investigation, Writing – original draft, Conceptualization. **Mohamed A. Ettabib:** Validation, Supervision, Writing – review & editing. **James S. Wilkinson:** Funding acquisition, Conceptualization, Supervision, Writing – review & editing. **Michalis N. Zervas:** Supervision, Conceptualization, Writing – review & editing, Writing – original draft.

Declaration of Competing Interest

The authors declare that they have no known competing financial interests or personal relationships that could have appeared to influence the work reported in this paper.

Data availability

Data underlying the results presented in this paper are available in Dataset DOI https://doi.org/10.5258/SOTON/D2516.

Acknowledgements

This work was funded by the U.K. Engineering and Physical Sciences Research Council (EPSRC) under Grant EP/ R011230/1, "Flexible Raman biosensing platform for low-cost health diagnostics". Z.L. acknowledges financial support from the China Scholarship Council (Grant No. 201808430227).

Appendix

Transmittance/reflectivity across the multilayer is calculated with the transfer matrix method, including the standard case that the source is incident from outside the optical layers and the case that the source is dipole radiation from inside the optical layers, and detailed as follows.

Ref. [12] has given the solution for field distribution of the dipole radiated from a three-layer system, however, here, the solution for the four-layer system that was discussed in the main text will be found from a generalized n-layer system.

Standard transfer matrix method for calculating the multilayer structure illustrated in Fig. 6(a) is given in Ref. [10,15]:

Light transfer in the same layer n from y_{n-1} to y_n is expressed as

$$\begin{bmatrix} A_n' \\ B_n' \end{bmatrix} = M_n \begin{bmatrix} A_n \\ B_n \end{bmatrix} \tag{10}$$

where the transfer matrix for layer n is

$$M_n = \begin{bmatrix} e^{i\phi_n} & 0 \\ 0 & e^{-i\phi_n} \end{bmatrix}. \tag{11}$$

in which ϕ_n is the phase shift in layer n due to propagation.

The matrix for light propagating across the interface n/n + 1 can be written as

$$M_{n,n+1} = \frac{1}{t_{n,n+1}} \begin{bmatrix} r_{n,n+1} & 1 \\ 1 & r_{n,n+1} \end{bmatrix} \tag{12}$$

The transfer matrix describes the light transfer from layer n to n + 1 is

$$\begin{bmatrix} A_n \\ B_n \end{bmatrix} = \boldsymbol{M}_{n,n+1} \begin{bmatrix} A_{n+1} \\ B_{n+1} \end{bmatrix} \tag{13}$$

where $\mathbf{M}_{\boldsymbol{n},\boldsymbol{n}+1} = \boldsymbol{M}_n \boldsymbol{M}_{n,n+1}$.

The transfer matrix for the whole structure is the product of all matrixes for each layer

$$\begin{bmatrix} R \\ 1 \end{bmatrix} = \widetilde{\boldsymbol{M}} \begin{bmatrix} 0 \\ T \end{bmatrix} \tag{14}$$

where 1 in the vector is the unit input as shown in Fig. 6(a), and

$$\widetilde{\boldsymbol{M}} = \prod_{i=0}^{n} \boldsymbol{M}_{n,n+1} \tag{15}$$

is the transfer matrix for the whole structure, i.e.

$$\begin{bmatrix} R \\ 1 \end{bmatrix} = \begin{bmatrix} \widetilde{M}_{00} & \widetilde{M}_{01} \\ \widetilde{M}_{10} & \widetilde{M}_{11} \end{bmatrix} \begin{bmatrix} 0 \\ T \end{bmatrix} \tag{16}$$

and consequently

$$T = \frac{1}{\widetilde{M}_{11}}, \; R = \frac{\widetilde{M}_{01}}{\widetilde{M}_{11}} \tag{17}$$

R and T are the reflectivity and transmissivity for the whole structure from layer 0 to layer n.

The transfer matrix can also be applied for the calculation of the propagating constant β of the guided mode of the surface wave in the layers simply by find the singular z component of the wavevector letting [10]:

$$\widetilde{M}_{11} = 0 \tag{18}$$

For the structure with the input source located inside the dipole located within the layers, the electric field in the first and the last layer are $e_0 = [\mathbf{E_r}, 0]^T$ and $e_n = [0, \mathbf{E_t}]^T$, so the transfer matrix is

$$e_0 = \widetilde{M}\, e_n \tag{19}$$

Assuming the dipole is located at y_0 in the grating layer, the electric field is not continuous and the expression connecting the lower (y_0^-) and upper limits (y_0^+) around the dipole is (similar expression in Ref. [12]):

$$e_1(y_0^+) = \begin{bmatrix} v_+ \\ -v_- \end{bmatrix} + e_1(y_0^-) \tag{20}$$

The dipole induced electric field through the multilayer after multiple reflection is, in terms of transfer matrix, following Ref. [12]:

$$\begin{aligned} e_0(0) &= M_{01} M_1(-y_0) e_1(y_0^+) \\ e_1(y_0^-) &= M_1(y_0 + y_1) \boldsymbol{M_{1n}} e_n(y_n) \end{aligned} \tag{21}$$

Then we can use (20) and (21) to derive the connection between the dipole generated field in the upper and lower side of the multilayer

$$\begin{bmatrix} \boldsymbol{E_r} \\ 0 \end{bmatrix} = \boldsymbol{M_{01}} M_1(-y_0) \begin{bmatrix} v_+ \\ -v_- \end{bmatrix} + \widetilde{\boldsymbol{M}} \begin{bmatrix} 0 \\ \boldsymbol{E_t} \end{bmatrix} \tag{22}$$

Thus, the up and down going electric field can be easily found as

$$\begin{aligned} \boldsymbol{E_t} &= \frac{1}{t_{01}} \left(v_- e^{-i\phi_0} - r_{01} v_+ e^{i\phi_0} \right) \Big/ \widetilde{M}_{11} \\ \boldsymbol{E_r} &= \frac{1}{t_{01}} \left(-r_{01} v_- e^{-i\phi_0} + v_+ e^{i\phi_0} \right) + \widetilde{M}_{01} \boldsymbol{E_t} \end{aligned} \tag{23}$$

where $\pm i\phi_0$ is the phase shift for the up and down going wave from y_0 to lower 0–1 interface. Eq. (23) is the general expression for the dipole at y_0 induced electric field at both upper and lower sides of the n-layer structure. For the four-layer structure in our main text, the solution can be simply found by replacing the subscripts 0–3 with a, g, f and s for the transfer matrices. Since $\boldsymbol{M}_{ij}\boldsymbol{M}_{ji} = \boldsymbol{I}$, where $\boldsymbol{I}$ is the 2x2 unit diagonal matrix, Eq. (22) can be rewritten as

$$M_g(y_0)M_{ga}\begin{bmatrix} \boldsymbol{E}_a^+ \\ 0 \end{bmatrix} = \begin{bmatrix} v_+ \\ -v_- \end{bmatrix} + \boldsymbol{M}_{gs}\begin{bmatrix} 0 \\ \boldsymbol{E}_s^- \end{bmatrix} \tag{24}$$

By replacing the matrix element with corresponding reflectivity/transmissivity and phase shift indicated in Eqs. (12) and (17), an expression with clearer physical meaning is found as

$$\begin{aligned} E_s^-(y_0,k_z) &= \frac{T_{gs}e^{+ik_{yg}\sigma}\left(v_+ r_{ga}e^{-i\Phi_0} + v_- e^{+i\Phi_0}\right)}{1 - r_{ga}R_{gs}e^{+i2k_{yg}\sigma}} \\ E_a^+(y_0,k_z) &= \frac{t_{ga}e^{+ik_{yg}\sigma}\left(v_+ e^{-ik_{yg}\sigma}e^{-i\Phi_0} + v_- R_{gs}e^{+ik_{yg}\sigma}e^{+i\Phi_0}\right)}{1 - r_{ga}R_{gs}e^{+i2k_{yg}\sigma}} \end{aligned} \tag{25}$$

References

[1] Cheng L, Mao S, Li Z, Han Y, Fu H. Grating Couplers on Silicon Photonics: Design Principles. Emerg Trends Practical Issues Micromach 2020;11:666. https://doi.org/10.3390/mi11070666.

[2] Ettabib MA, Liu Z, Zervas MN, Wilkinson JS. Optimized design for grating-coupled waveguide-enhanced Raman spectroscopy. Opt Express 2020;28:37226. https://doi.org/10.1364/oe.410602.

[3] Sychugov VA, Tishchenko AV, Lyndin NM, Parriaux O. Waveguide coupling gratings for high-sensitivity biochemical sensors. Sens Actuators B 1997;39:360–4. https://doi.org/10.1016/S0925-4005(97)80234-1.

[4] Tamir T. Integrated Optics (Topics in applied physics; v. 7). New York: Springer-Verlag Berlin Heidelberg; 1975. https://doi.org/10.1007/978-3-662-43208-2.

[5] Dalgoutte DG, Wilkinson CDW. Thin grating couplers for integrated optics: an experimental and theoretical study. Appl Opt 1975;14:2983. https://doi.org/10.1364/ao.14.002983.

[6] Wohlfeil B, Zimmermann L, Petermann K. Optimization of fiber grating couplers on SOI using advanced search algorithms. Opt Lett 2014;39:3201. https://doi.org/10.1364/ol.39.003201.

[7] Payne FP, Lacey JPR. A theoretical analysis of scattering loss from planar optical waveguides. Opt Quant Electron 1994;26(10):977–86.

[8] Schmid JH, Delâge A, Lamontagne B, Lapointe J, Janz S, Cheben P, et al. Interference effect in scattering loss of high-index-contrast planar waveguides caused by boundary reflections. Opt Lett 2008;33(13):1479.

[9] Tamir T, Peng ST. Analysis and Design of Grating Couplers. Appl Phys 1980;21:410. https://doi.org/10.1007/BF00895934.

[10] Yeh P. Optical Waves in Layered Media. Wiley; 2005.

[11] Bracewell RN, Bracewell RN. The Fourier transform and its applications, vol. 31999. New York: McGraw-Hill; 1986.

[12] Sipe JE. New Green-function formalism for surface optics. J Opt Soc Am B 1987;4:481. https://doi.org/10.1364/josab.4.000481.

[13] Brent RP. Algorithms for minimization without derivatives. Courier Corporation 2013.

[14] Virtanen P, Gommers R, Oliphant TE, Haberland M, Reddy T, Cournapeau D, et al. SciPy 1.0: Fundamental Algorithms for Scientific Computing in Python. Nat Methods 2020;17(3):261–72.

[15] Byrnes SJ. Multilayer optical calculations. ArXiv:160302720 2016:1–20.